

LETTER TO THE EDITOR

The Discovery of Transitive Phenomenon in the Radio Emission of the mode-switcher PSR B0943+10

S. A. Suleymanova¹ and A. V. Bilous²

¹ P. N. Lebedev Physical Institute of the Russian Academy of Sciences, Pushchino Radio Astronomy Observatory, Pushchino 142290, Russian Federation

² ASTRON, the Netherlands Institute for Radio Astronomy, Postbus 2, 7990 AA Dwingeloo, The Netherlands

October 11, 2022

ABSTRACT

PSR B0943+10 is known to switch between two distinct, hours-long modes of radio emission, Bright (B) and Quiet (Q). Up to now the switches in both directions were believed to occur instantly (on the scale of a spin period). We have found a transitive process around the Q-to-B-mode switch, which consists of two additional short-lived modes, each with distinct average profiles and subpulse drift rates. Based on observations at low radio frequencies, we examine the properties of these transitive modes and discuss their implications in the framework of the traditional carousel model of drifting subpulses.

Key words. pulsars – individual sources PSR B0943+10

1. Introduction

PSR B0943+10 is a classical example of the so-called “mode-switching” pulsars, a small subset of radio pulsars that switch between several stable states of the electromagnetic emission. For PSR B0943+10, two modes have been identified so far: “Bright” (or “Burst”) and “Quiet” (hereafter B-mode and Q-mode, see Suleymanova & Izvekova 1984). In radio band, both the average pulse shape and the properties of single-pulse emission change between the modes, with B-mode being notorious for the organized temporal drift of individual subpulses (e.g. Deshpande & Rankin 2001).

In the X-ray band, the radio mode switch is accompanied by changes in average pulse morphology and flux density (Hermsen et al. 2013; Mereghetti et al. 2016). The X-ray emission in both modes has a pulsed thermal component originating in the hot polar cap region on the neutron star surface, few hundred kilometers away from the presumable origin of the magnetospheric radio emission (Bilous et al. 2014). Thus, some global-scale magnetospheric transformation is expected during mode transitions (Timokhin 2010; Cordes 2013).

Studying the properties of mode transitions may help constraining the nature of said transformation and the searches for peculiar single-pulse behavior around mode switches have been conducted regularly. To the extent of authors’ knowledge, no such effects have been found so far: recorded mode transitions happen instantly and abruptly (Bartel et al. 1982; Wang et al. 2007; Esamdin et al. 2005; Rajwade et al. 2021).

For PSR B0943+10 mode transitions have been considered to be instantaneous as well, although there is no clear corroboration of this in the published literature. In this paper we report the discovery of transitive phenomena around Q-to-B mode switches in several archival low-frequency observations conducted at 112 MHz with Large Phased Array (LPA) at Pushchino Radio Observatory (PRAO), and at 25–80 MHz with the LOw-Frequency ARray (LOFAR, van Haarlem et al. 2013). This tran-

sitive state (hereafter T-mode) lasts for about 1 minute or 60 pulsar rotations, thus being much shorter than the hours-long main modes. We describe the peculiar single-pulse properties during T-mode and speculate on their implications for the mode switching theories.

2. Observations and data processing

2.1. PRAO

LPA is a transit instrument and the duration of observing session can not exceed $3.5 \text{ min}/\cos \delta$, where δ is the declination of the source. For PSR B0943+10, with its spin period $P_1 = 1.0977 \text{ s}$, this translates to a maximum of 194 pulses available per session. The pulses were recorded using a digital receiver with a bandwidth of 2.5 MHz divided into 512 4.88-kHz spectral channels by a Fast Fourier Transform (FFT) processor. The actual total bandwidth taken into processing was 2.245 MHz. The signal was dedispersed to the frequency of 111.88 MHz (hereafter 112 MHz).

The narrow bandwidth of the channels reduced the effect of pulse broadening caused by interstellar dispersion delay. At 112 MHz the total pulse delay within a single channel for PSR B0943+10’s DM of 15.4 pc cm^{-3} is 0.5 ms, much smaller than the time resolution of 2.8672 ms. More detailed description of LPA’s digital receiver and data pre-processing is given in Suleymanova et al. (2012).

With a rotation measure of $15 \pm 1 \text{ rad/m}^{-2}$ (Suleymanova et al. 1998), the Faraday modulation period at 112 MHz is about 1.6 MHz, which is comparable to the total bandwidth of the receiver. Thus, despite LPA being a linearly polarized array, the recordings provide a reasonable estimate of the pulsar’s total intensity emission (see also Suleymanova & Rankin 2009).

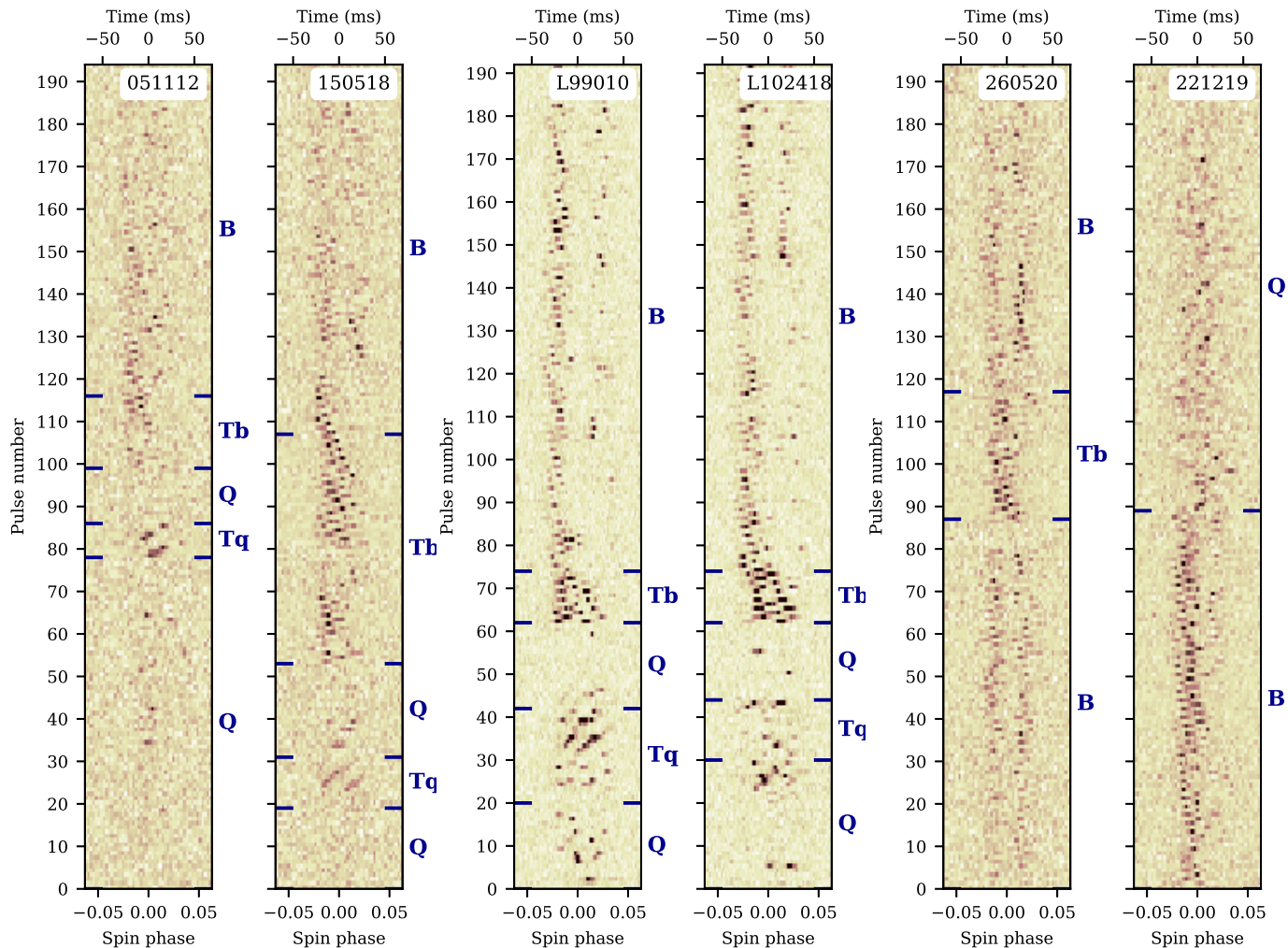


Fig. 2. Single-pulse sequences for six observing sessions at LPA (112 MHz) and LOFAR (30–80 MHz) telescopes. The designations for sessions at LPA are given in *ddmmyy* format. Observations with IDs starting with L were taken at LOFAR. For all sessions only the on-pulse region is shown and the colors are saturated to highlight fainter pulses. Mode boundaries were determined based on the average profile morphology and the presence of subpulse drift in 2D FFT spectra (Sect. 4.2.1). Sessions 051112, 150518, L99010 and L102418 feature Q-to-B mode transitions. Session 260520 shows a rare B-Tb-B mode transition and 221219 exhibits a typical featureless B-to-Q mode switch.

characteristic time of about 73 min. The change is faster at B-mode onset. Later it was found that this behavior is independent of observing frequencies between 40 and 327 MHz and over the timescale of several years (Rankin & Suleymanova 2006; Backus et al. 2011; Suleymanova & Pugachev 2017; Bilous 2018; Suleymanova et al. 2021).

In turn, emission in the Q-mode is stable in the sense that no gradual changes in its properties have been recorded. Despite systematic searches, no drifting subpulses have been detected in the Q-mode (Suleymanova & Izvekova 1984; Backus et al. 2010), except for an occasional feature at 0.0275 cycles/ P_1 corresponding to $\hat{P}_3 = 36.4P_1$ (Rankin & Suleymanova 2006). The origin of this feature is unclear and no similar features have been found since then (Bilous 2018).

3.2. Average profile

In both modes the average pulse profile is composed of two components of equal width which are moving away from each other

at lower frequencies. The full width at half maximum of the components is about 7:2 for the B-mode and 11:5 in Q-mode and does not show a strong dependence on frequency between 40 and 80 MHz (Bilous et al. 2014). Recently Suleymanova et al. (2021) have shown that the width of the average pulse components in the B-mode is constant over the wider frequency range of 62–1391 MHz with the separation between components increasing rapidly towards lower frequencies in accordance with a power law:

$$s(^{\circ}) = 130^{\circ}8 \times \nu_{\text{MHz}}^{-0.56}.$$

In B-mode the leading component is generally brighter than the trailing one, however the ratio of components' peak amplitudes changes in a frequency-dependent manner as the mode evolves. For the first few minutes of the B-mode, the trailing component may be brighter, again in a frequency-dependent manner. The fiducial longitude (midpoint between profile components, corresponding to the moment of time when the line-of-sight (LOS) passes closest to the magnetic axis) is systematically

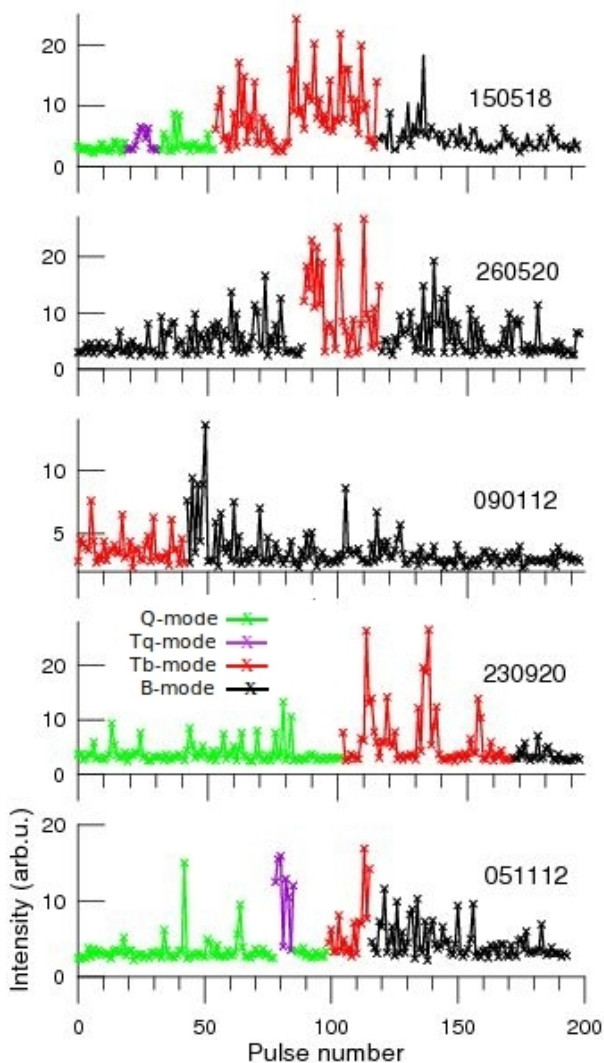


Fig. 3. Five records of Q-to-B mode switches from the archives of 112-MHz observations. The intensity of subpulses in units of signal-to-noise ratio is given as a function of pulse number. Individual modes are highlighted with different colors (black for B-mode, green for Q-mode, red for Tb-mode, and magenta for Tq-mode).

delayed by about 1:4 per mode, resetting at the next Q-to-B transition. The amplitude of delay does not depend on frequency at least between 40 and 327 MHz (Bilous et al. 2014; Suleymanova et al. 2021). No such effect has been identified for Q-mode.

4. The transitive phenomenon around Q-to-B transition

4.1. Identification of the Tb- and Tq-modes

Figure 2 shows examples of individual pulse sequences for some of our observations. In general, the difference between the B- and Q-modes is evident to the naked eye. In the B-mode, individual pulses form two columns corresponding to components of the average profile. The drift of subpulses near central longitudes is not visible due to a decrease in average pulse intensity in the saddle between the components. In the Q-mode subpulses are distributed randomly within the on-pulse window.

Panels 150518, L99010, L102418 and 260520 show unusual behavior of subpulses around Q-to-B mode transitions. When

subpulse drift recommences after the end of Q-mode, for a short period of time subpulses drift through entire on-pulse window and, unlike later on, there is no fading of subpulses at central longitudes. During this period the on-pulse window is somewhat narrower than in well-established B-mode sequences.

These features allowed us to identify these particular sequences of pulses as a new mode, which we designated “Transitive B-like” mode, or Tb-modes. Tb-mode has been recorded in all available observations except for session L169237 in Bilous et al. (2014). Comparing with the sessions presented on Fig. 2, the S/N ratio of the pulsed signal is smaller there, and emission is modulated by scintillation, with one of the intensity troughs coinciding with Q-to-B transition (see Fig. 1 in Bilous et al. 2014).

On panel 260520, the subpulse drift pattern characteristic to Tb-mode is observed in the 30-second interval between B-mode pulses. There are no Q-mode pulses in this record, but the shape of the average B-mode pulse profile, with two equally bright components, indicates that the Q-to-B switch occurred a few minutes before the start of observing session (Rankin & Suleymanova 2006; Suleymanova & Rankin 2009). The presence of Tb-mode pulses within the B-mode sequence suggests that B-mode emission in the first minutes after mode onset is unstable.

The Tb-mode is not the only transitive phenomenon around Q-to-B switches. Some time before Q-mode cessation there appear groups of pulses that slowly drift towards the trailing edge of the on-pulse window. This drift is present in all but one Q-to-B transitions observed. We have labeled these slowly drifting pulses as Transitive Q-like modes, or Tq-modes.

Both Tb- and Tq-modes exhibit drifting subpulses and the presence of this drift was used to establish mode boundaries. However, the Tb-mode does not follow Tq-mode immediately. Between them there is a gap of several spin periods with very scarce single pulses resembling those of the Q-mode. Interestingly enough, the only observed B-Tb-B transition also exhibits the absence of emission for a few seconds before the Tb-mode starts (Fig. 2, panel 260520).

Because the transit time of PSR B0943+10 through the BSA beam is much smaller than the typical duration of its main modes, the records of mode switching are rare, with only five sessions with Q-to-B transitions being found in the archives. Subpulse intensities for these five records are shown in Fig. 3, with different modes shown by different colors. There are no Q-mode pulses in the 090112 session. The low values of the subpulse drift rate indicated that the first 42 pulses correspond to the Tb-mode, and the remaining pulses to the B-mode. In addition, the shape of the averaged pulse in B-mode with the ratio of components $R(2/1) = 2.1$ clearly pointed out to the Q-to-B switch occurring shortly before the start of the observation session (Rankin & Suleymanova 2006; Suleymanova & Rankin 2009).

In five cases on Fig. 3 the Tq-mode is much shorter than the Tb-mode, and in one session (230920) it is absent completely. The duration of the Tb-mode varies between sessions, comprising 17–66 spin periods or 19–69 s. At lower frequencies, the two transitions recorded exhibit shorter Tb-modes – only 13 s, however this may be just a coincidence. More low-frequency observations are needed to explore the Tb-mode duration below 100 MHz.

To our surprise, the opposite, B-to-Q mode transitions were featureless (e.g. panel 221219 on Fig. 2). No transitive phenomena were found in any of our recordings.

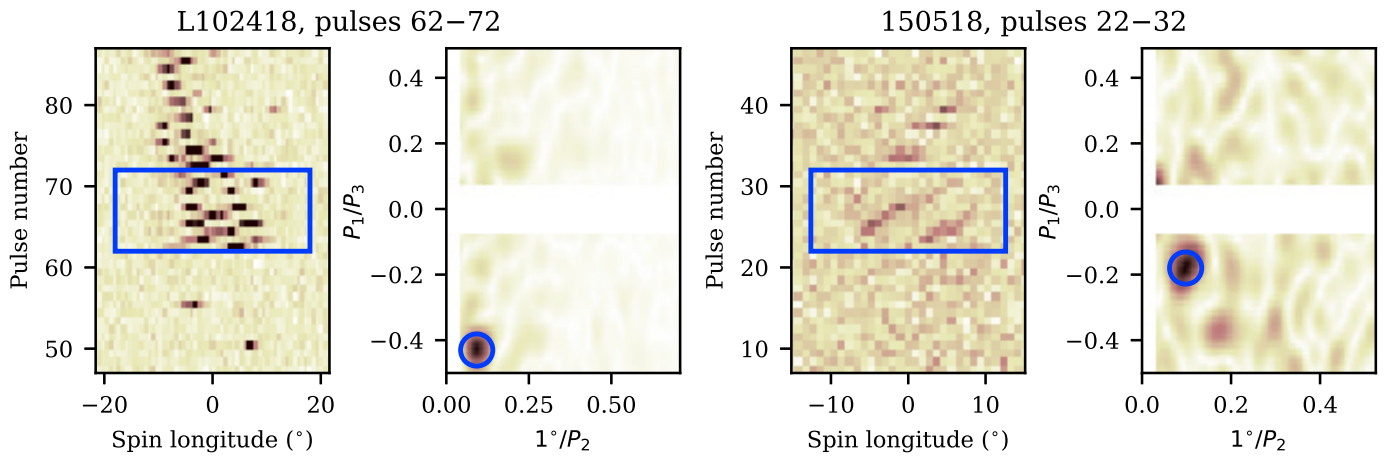


Fig. 4. An example of a 2D (spin longitude vs pulse number) FFT spectrum featuring the Tb-mode of session L102418 (left) and Tq-mode of session 150518 (right). The Fourier transform was taken from the region enclosed in the blue rectangle on the left-side pulse sequence plot. Frequencies close to zero were eliminated from analysis to reduce the influence of red noise on the peak finding algorithm. The colorbar range in each figure is set by the local minimum and maximum and is not uniform across different LRF spectra.

4.2. Subpulse drift

4.2.1. Tb- and Tq-modes

Both Tb- and Tq-modes are much shorter than pulse sequences typically used for computing LRF spectra and determining drift parameters in the B-mode. Cutting the usual few-hundred pulse sequences around Tb- and Tq- modes pollutes the spectra with either B-mode drift or Q-mode noise, diminishing the S/N of the transitive mode spectra peaks, which is detrimental for the fainter Tq-mode sequences. However, finding peaks on LRF spectra usually involves integrating spectral power within on-pulse window, thus not taking into account the regularity of the longitude separation between subpulses in the same period (this information is stored in the complex phase of LRF spectra). The 2D FFT transform (Edwards & Stappers 2003) does not have this disadvantage and thus is better suited for measuring the drift parameters of the short pulse sequences of the Tq- and Tb-modes.

To measure \hat{P}_3 and P_2 simultaneously, we performed 2D FFT transforms in a fixed-size window sliding along the pulse number axis. The window size was 10 pulses by 22° or 40° of rotational longitude for LPA and LOFAR observations, respectively. The sliding step was $2P_1$. In order to measure the position of FFT peak more precisely, sequences of zeros were added to each data row, boosting the nominal Fourier frequency resolution by a factor of 10. Formal errors on \hat{P}_3 and P_2 were derived from the frequency resolution of the padded data transforms, however the real, noise-influenced errors are supposed to be larger by a factor of a few.

To estimate the significance of recorded features we performed the same feature extraction procedure on original pulse sequences but with randomized subpulse positions. The randomization was done by shuffling the pulse periods within the groups of 4 phase bins. This way the average shape of 10-pulse integrations was preserved, while destroying any periodicity along the axis of constant longitude and attenuating the periodicity in orthogonal direction. This procedure was performed 1000 times and the percentile of peak on FFT spectrum of the real data was compared to the distribution of the corresponding peaks of the simulation. Given the total length of the pulse sequences explored, the total number of chance detections above our threshold is estimated to be between 0.5 (independent 10-pulse sequences) and 6 (independent 2-pulse sequences).

Examples of 2D FFT spectra are given on Fig. 4. Most of the features detected came from Tb- and B-modes where subpulse drift is visible to the naked eye. In all but one sessions there had been significant detections of drift periodicity in the Q-mode short before the Q-to-B transition (Tq-mode). In both transitive modes, as well as in the B-mode the feature at positive \hat{P}_2 had negative \hat{P}_3 , meaning that pulses drifted to the trailing edge of the onpulse window.

\hat{P}_3 in the Tq-mode varies substantially between mode instances, ranging from approximately $3.2P_1$ to $6.7P_1$. It also exhibits variation within the Tq-mode itself. For the Tb-mode \hat{P}_3 stays closer to the B-mode values, most of the times being larger than in the B-mode. The jitter of measured \hat{P}_3 in the B-mode is partially due to noise influence, and partially intrinsic – in Bilous (2018) LRF spectra on 512-pulse sequences recorded multiple peaks with frequency spread on the order of $0.01P_1/P_3$.

Interestingly enough, the subpulse separation remains more or less constant throughout Tq-, Tb- and B-modes, varying chaotically around 11° with a magnitude of $1^\circ - 2^\circ$. P_2 for the same LOFAR sessions was also measured in Bilous (2018) using a more precise phase track method on 512-pulse sequences, which takes into account the observed increase of subpulse separation at the edge of the onpulse window due to the curved LOS path. In their work P_2 at the fiducial longitude (middle of onpulse window for PSR B0943+10) is $10:6 - 10:8$, with $P_2 \approx 18^\circ$ at $\pm 15^\circ$ of spin longitude. In our case, the 2D FFT gathers information from the entire onpulse window, thus our P_2 is larger. Since pulse sequences comprise only 10 pulses, the illumination of the onpulse window is quite uneven, bringing extra variability in measured P_2 .

4.2.2. Comparing drift properties in Tb- and B-modes

The shape of the average pulse changes abruptly during Tb-to-B transition, however the evolution of drift parameters seems to be smooth. It is interesting to compare $f_3 \equiv |P_1/\hat{P}_3|$ in the Tb-mode to the global evolution of f_3 during the B-mode. At 112 MHz we used a Discrete Fourier Transform to calculate f_3 for short sequences of pulses of the transitive modes. In some cases we were forced to calculate f_3 on longer pulse sequences which included non-modulated Q-mode emission. For the LOFAR data

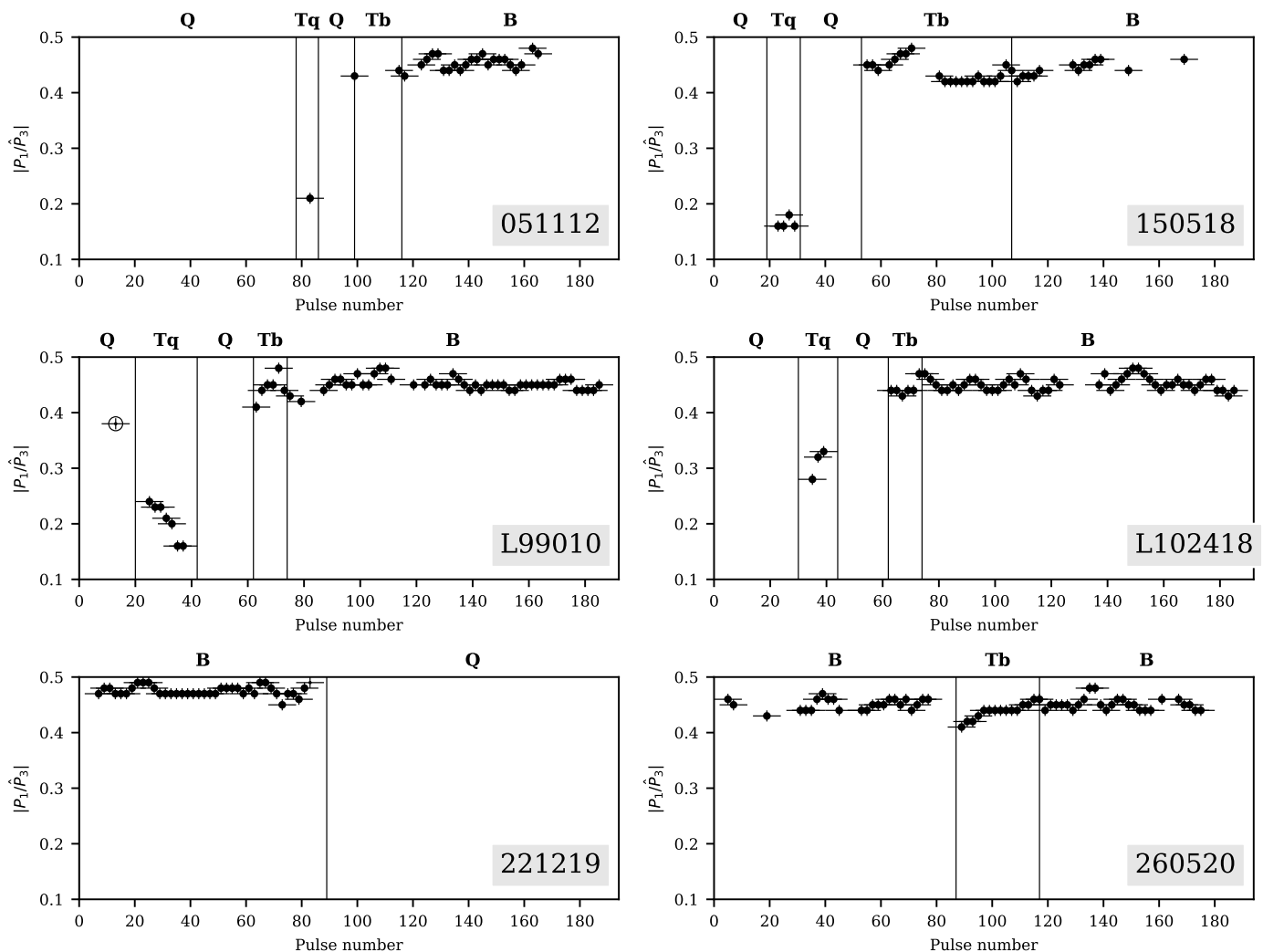


Fig. 5. The absolute value of the modulation frequency around the lines of constant spin phase ($f_3 \equiv |P_1/\hat{P}_3|$) as a function of time for the pulse sequences from Fig. 2. Horizontal errorbars mark the edges of 10-pulse samples used for f_3 calculation. Vertical errorbars show the nominal frequency determination error taking into account the zero-padding. For each subsample, only f_3 with the highest S/N is plotted (see text for details on S/N estimates). Only peaks which were stronger than 99.5% of the simulated sample are shown. The vertical lines mark mode edges. All points here correspond to negative \hat{P}_3 except for the hollow one for session L99010. For the PRAO sessions, the absence of f_3 points near the observation end is due to pulsar signal attenuation.

we used mean values of the Tb-modes from Fig. 5, with the errorbar corresponding to the standard deviation of f_3 .

Examples of onpulse-integrated LRFS for three such longer 91-pulse sequences observed at 112 MHz are shown in Fig. 6 for the Tb-mode (session 150518), early B-mode (session 260520), and late B-mode (221219). Each spectrum is normalized by the peak amplitude for clarity. The features corresponding to frequencies $f_3 = 0.428, 0.449,$ and 0.472 cycles/ P_1 , respectively, are narrow and well resolved¹. It is obvious that f_3 gradually increases throughout the combined Tb- and B-modes.

A larger compilation of f_3 measurements is shown in Fig. 7. It comprises the f_3 values for the Tb- and B-modes from the current work, as well as LOFAR B-mode measurements from Bilous (2018), and Arecibo 327-MHz values from Rankin & Suleymanova (2006). As indicated in these studies and in Backus et al. (2011), the frequency of the amplitude fluctuations varies with time according to the exponential law (dashed line), where

¹ Note that for the Tb-mode some excess power is present at f_3 going up to 0.5 cycles/ P_1 , corresponding to higher f_3 during the first half of the Tb-mode for session 150518 in Fig. 5.

t is the time since mode onset (min):

$$f_3 = 0.471 - 0.022 \times e^{-t/73}. \quad (4)$$

This equation limits f_3 to the range of 0.449 – 0.471 cycles/ P_1 . Numerous observations of PSR B0943+10 at 112 MHz showed that for roughly 2.5% of B-mode pulse sequences $f_3 < 0.449$ cycles/ P_1 . Thus, Suleymanova & Pugachev (2017) have proposed a better power-law parametrization that encompasses all B-mode f_3 measurements:

$$f_3 = 0.439 \times t^{0.0126}. \quad (5)$$

In the Tb-modes, f_3 varies in the range of 0.428–0.439 cycles/ P_1 with a mean value of 0.434 ± 0.004 cycles/ P_1 that is significantly lower than has ever been measured for the B-mode. Nevertheless, these values can be considered as compatible with the power law f_3 -time dependence in the B-mode. For both functions in Fig. 7, $t = 0$ at B-mode onset. During the Tb-mode $t < 0$, thus its f_3 values were not included in the power-law fitting procedure. The average value of f_3 at B-mode onset following the Tb-mode is 0.449 ± 0.002 cycles/ P_1 , as it was expected.

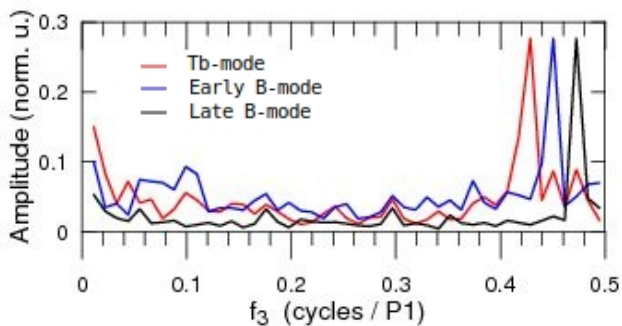


Fig. 6. Examples of onpulse-integrated LRF spectra calculated for 91-pulse sequences containing the Tb-mode (150518, red line), early B-mode (260520, blue line), or late B-mode (221219, black line). Corresponding frequencies are 0.428, 0.449, and 0.472 cycles/ P_1 .

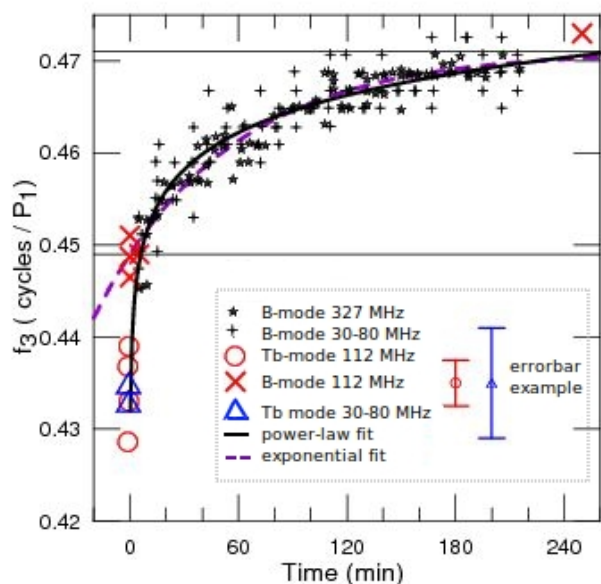


Fig. 7. A compilation of observed f_3 values as a function of time since B-mode onset. Previously published f_3 measurements are shown by black stars (Arecibo, 327 MHz) and black crosses (LOFAR, 30–80 MHz). The 112-MHz measurements for the Tb- and B-modes from this work are shown with red circles and crosses. The f_3 value for 91 B-mode pulses right before a B-to-Q mode transition (session 221219) is plotted at an arbitrary time mark of 250 min. LOFAR Tb-mode f_3 measurements are shown with blue triangles. The points around $t = 180$ min show typical f_3 errorbars for PRAO and LOFAR measurements from this work. Horizontal lines mark the range of validity of the exponential fit by Backus et al. (2011, dashed magenta line). The black line shows power-law fit from Suleymanova & Pugachev (2017). The measurements for the Tb-mode are in a good accordance with a power law fit.

4.3. Average pulse profile during transitive modes

Figure 8 shows the average profiles for all four modes in two LOFAR sessions with Q-to-B transition. The shape of the average profile in transitive modes varies between the sessions and is dominated by the individual strong pulses. Given the small number of modes and their relative shortness, it is hard to compare the average profiles in transitive modes with the regular B- and Q-modes, however it can be stated that neither the Tq- nor Tb-mode exhibit two distinct separate components like the B-mode.

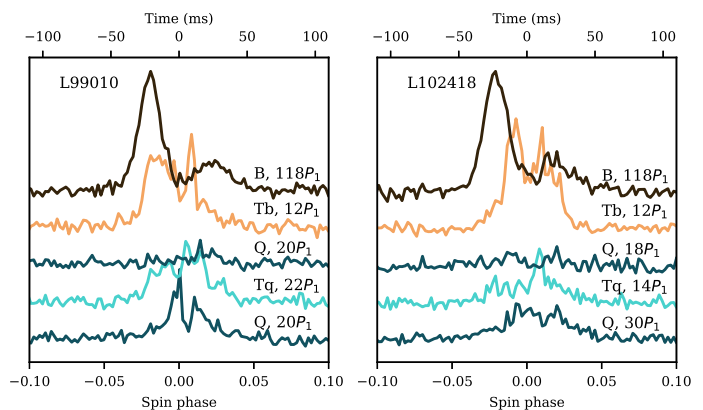


Fig. 8. Average profiles integrated within the respective modes for two LOFAR sessions with Q-to-B transitions normalized by the standard deviation of signal outside the on-pulse window.

PRAO observations offer larger mode samples and, also, longer instances of the Tb-mode. Figure 9 shows the average profiles integrated within B- and Tb-modes for the three PRAO sessions which exhibited prominent B-mode component peaks to facilitate alignment between sessions. The bottom panel presents integrated profiles for these three sessions, comprising 135 individual pulses for the Tb-mode and 390 pulses for the B-mode. It is evident that at 112 MHz the Tb-mode has no separate components and the profile is asymmetric and skewed to earlier spin longitudes.

Interestingly, the shape of the pulse profile in the averaged Tb-mode closely matches the composite Q+B profile recorded close to the B-to-Q transition (session 221219, Fig. 10a, b). In the session 221219, the B-to-Q switch happened in the middle of the observation. For comparison, the average Tb-mode profile from Fig. 9 was shifted by 5.7 ms toward earlier spin longitudes. This close resemblance of the pulse shapes could indicate that around the Q-to-B switch the regions responsible for the Q- and B-modes emit simultaneously and that their contribution is equal. This is possible only under the condition that the B- and Q-pulses are emitted from two independent regions in the pulsar magnetosphere. In the core/cone model (Rankin 1983), the Q- and B- modes in PSR B0943+10 are associated with the core and conal beams of emission which emit alternately. The discovery of the transitive modes allow us to suggest that over some short time these two independent regions may emit simultaneously.

If the Tb-mode emission is indeed a superposition of the Q- and B-modes, then the 5.7 ms delay is naturally explained by the evolution of the on-pulse window location throughout the B-mode. It is known that during the lifetime of each B-mode instance, the average pulse shifts towards later longitudes. The total shift varies from 4 to 6 ms per B-mode duration (Bilous et al. 2014; Suleymanova & Rodin 2014; Suleymanova & Pugachev 2017). Thus, the Tb-mode emission is a superposition of late B-mode and the Q-mode. During the instantaneous Tb-to-B switch the emission window resets at earlier longitudes and the slow shift to the later longitudes continues during new B-mode instance. Within this interpretation it is hard to explain though the B-Tb-B sequence of the 260520 session, where both B-mode sequences framing the Tb-mode exhibited the properties of the early B-mode.

Observational evidence speaks against the Q-mode emission being produced by a core component in the core/cone model of the pulsar radio beam. First of all, this evidence includes the ap-

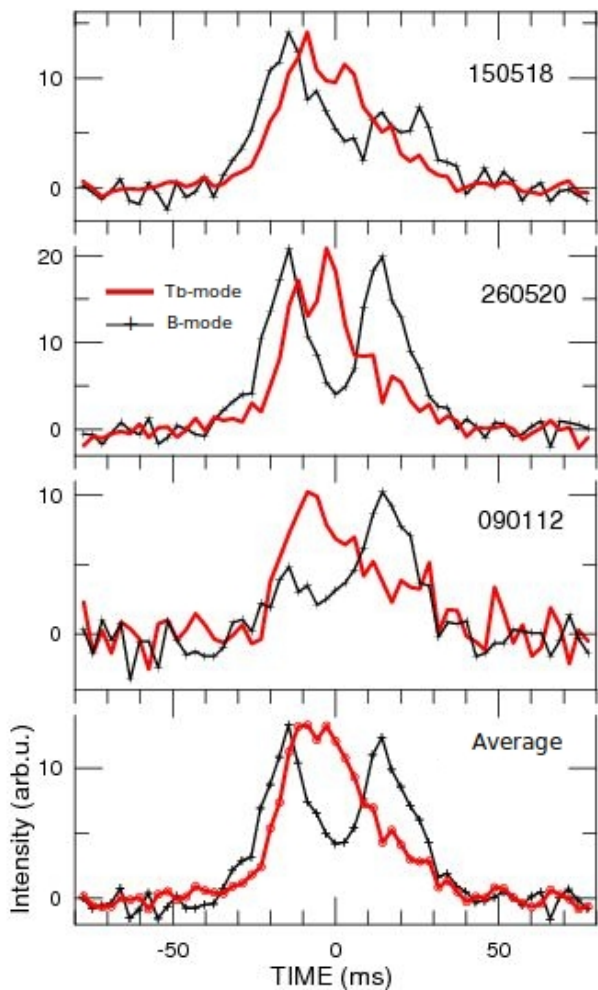


Fig. 9. Average pulse shape of the Tb-mode (red line) and the B-mode (black line with crosses) for sessions (from top to bottom) 150518, 260520, and 090112. Profiles for different days were aligned by the leading peak of B-mode profile. The lowest panel shows profiles averaged over these three sessions.

pearance of organized subpulse drift (Tq-mode) within the sequence of Q-mode pulses right before the Q-to-B switch and the crude similarities between the shapes of the average profile in both modes. Also, at frequencies lower than 100 MHz Q-mode profiles exhibit conal components that separate progressively (Suleymanova et al. 1998; Bilous et al. 2014). It was shown that for PSR B0943+10 the sightline makes only a grazing transverse of the polar cap (Deshpande & Rankin 2001) and the scenario in which the observer misses most of the core radiation because of this peripheral sightline was previously put forward to explain the relative faintness of PSR B0943+10’s radio emission during its bright X-ray mode (Hermsen et al. 2013; Rankin et al. 2020). Another scenario can be proposed in which core radio beam is missed completely and all modes observed in PSR B0943+10 originate from conal beam shape variations. These variations are correlated with $\mathbf{E} \times \mathbf{B}$ drift behaviour of the localized spark discharges.

Observations at 112 MHz show that the width of the on-pulse window stays similar throughout all four modes (Fig. 10). It is considered to be determined by the size of the polar cap with the radius R_{out} . Within the framework of the traditional core/cone model of pulsar radio emission (e.g. Rankin 1983, and other pa-

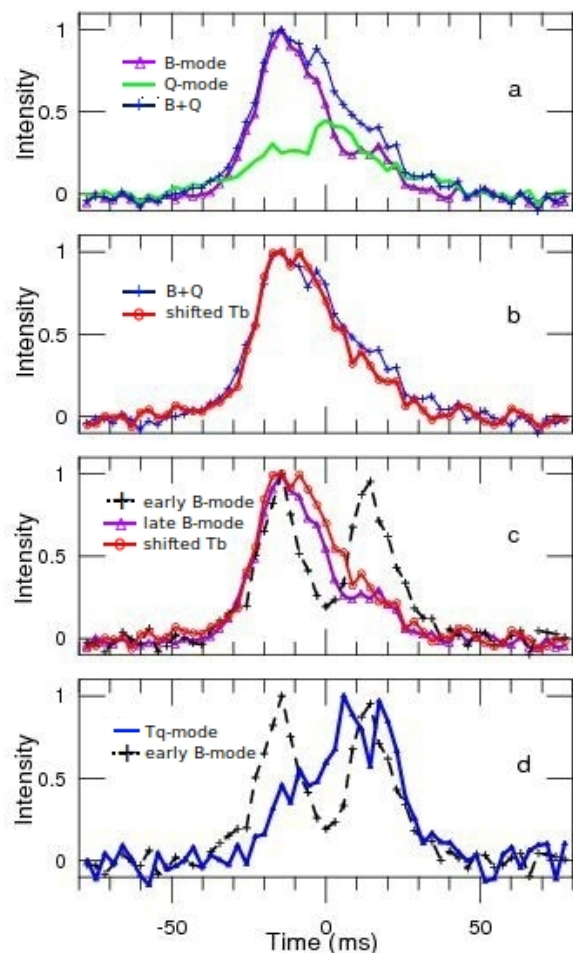


Fig. 10. (a): mode-separated average profiles for session 221219, where the B-to-Q transition occurred in the middle of the observation. Violet and green lines correspond to the B- and Q-modes, respectively, and the thin blue line shows composite B+Q profile. (b): B+Q profile (blue line) superposed on the average Tb-mode pulse profile (red line) shifted by 5.7 ms towards earlier spin longitudes. (c): the B-mode pulse shape evolution starting from its onset (session 260520, dotted line) up to cessation (session 221219, violet line), together with Tb-mode pulse (red line) shifted by 5.7 ms towards earlier spin longitudes. (d): Tq-mode profile (blue line) accumulated from sessions 150518 and 051112. The B-mode profile on 260520 is given for comparison. Profiles for different days were aligned by the leading peak of the B-mode profile.

pers in this series), the width of the conal components in the average pulse profile is set by the thickness of the pair-producing ring in the polar gap: $W_{\text{ring}} = R_{\text{out}} - R_{\text{inn}}$, where R_{inn} is the inner radius of the ring. We suggest that the transitions between modes are accompanied by variations in the inner radius. This can explain the gradual increasing of the component’s width over the B-mode lifetime and the appearance of drifting subpulses at the central longitudes in the Tb and Tq-modes. At B-mode onset the two components of the average pulse profile are well separated with intensity in the saddle region close to zero below 100 MHz. The width of the components is at its minimum and grows with B-mode age (Bilous et al. 2014). For the leading component 112 MHz, the width can increase by as much as 40% (Suleymanova & Rodin 2014). This effect is well demonstrated in Fig. 10c, where the profiles of the average pulse for the onset and the end of the B-mode are shown. The width of the first component at the level of half maximum increases from 15 to 24 ms,

i.e. by 60%. The same panel shows the profile of the average Tb-mode with the width of 30 ms. The total change in profile width between the Tb- and early B-mode is 100%. With such a significant increase in the width of W_{ring} , central longitudes become illuminated for our line of sight and we observe drifting subpulses close to fiducial longitude in transitive modes.

Figure 10d shows the Tq-mode profile obtained at 112 MHz after averaging 20 pulses using sessions 150518 and 051112. It is worth noting that because of the short duration of the mode its average profile is distorted by bright pulses. However, comparing the Tq-mode to the Q-mode profile (Fig. 10a) reveals similarity in profile shape as far as they are both skewed to the trailing side (unlike B-mode). Similar behaviour is observed in LOFAR data (Fig. 8).

5. Summary

In this work we report on the discovery of a transitive process which takes place for about a minute around a Q-to-B-mode switch. This process consists of two stages which we labelled Tb- and Tq- modes.

5.1. Tb-mode and its comparison to the B-mode.

1. This mode precedes the B-mode onset by 40 ± 25 s. The duration of the Tb-modes exhibit larger variations from one instance to another, ranging between $12P_1$ and $66P_1$.
2. Similarly to B-mode, the individual subpulses drift from the leading to trailing edge of the onpulse window, however the drift extends now through the whole onpulse window, including central spin longitudes.
3. The amplitude modulation frequency in the Tb-mode varies in the range of $0.428 - 0.439$ cycles/ P_1 with the mean value of 0.434 ± 0.005 cycles/ P_1 that is significantly lower than f_3 values measured for the B-mode. Nevertheless, these values are in accordance with the power-law f_3 evolution throughout B-mode.
4. The average pulse profile in the Tb-mode is skewed to the leading edge, similar to the B-mode, however it does not have resolved conal components.
5. Sometimes the Tb-mode happens within an early B-mode instance.

5.2. Tq-mode and its comparison to the Q-mode.

1. The Tq-mode occurs within the late Q-mode and, unlike the latter, has a specific subpulse drift pattern. This mode precedes the Tb-mode onset by 34 ± 7 s and lasts for about $10 - 22P_1$. In one session no Tq-mode was recorded, however the S/N of the recording was quite low.
2. As in the Tb- and B-modes, subpulses in the Tq-mode drift towards the trailing edge of the onpulse window. The drift frequency f_3 varies from 0.149 to 0.312 cycles/ P_1 from one observation to another, with sometimes large variation of f_3 within the mode.
3. The average pulse profile in the Tq-mode has a tendency to be skewed to the trailing edge which is characteristic of the Q-mode.

6. Discussion

Short-lived mode sequences have been previously observed from several pulsars, for example PSR B1859+17 (Rajwade et al.

2021), PSR J1326–6700 (Wen et al. 2020), PSR J1909–3744 (Miles et al. 2021), and others. The peculiarity of PSR B0943+10’s transitive modes lies in the fact that they usually appear in a 1-minute interval around the switch between the two main hours-long modes, the Q- and B-mode. Both modes show similarities to the main modes and are considered as submodes, which is reflected in their designation.

Gil & Sendyk (2000) argued that subpulse drift is observed when a quasi-central spark is formed at the local pole of a sunspot-like surface magnetic field. This fixed spark prevents other sparks from moving towards the pole, restricting their motion to slow drift around the pole. Although little is known about PSR B0943+10’s small-scale magnetic field configuration, we can qualitatively apply this model to PSR B0943+10’s mode sequences. During the Q-mode no central spark is formed, sparks are quickly moving towards magnetic pole and subpulses are observed at random onpulse longitudes. At the end of the Q-mode the anchor spark appears, causing Tq-mode sequences. The carousel rotates relatively slowly and exhibits a lot of variation from one mode instance to another, as well as within the Tq-mode, possibly reflecting fast-paced changes in the spatial or temporal variations of accelerating potential in the polar gap. Subpulses are seen in the central region of the on-pulse window, indicating a larger width of the carousel. Subpulses briefly disappear (except for may be a few pulses) during the null-like period between the Tq- and Tb-modes. During the Tb-mode the carousel width remains large, but then gradually decreases throughout the B-mode. The carousel rotation rate evolves in a similar manner, more rapidly during the Tb- and early B-mode and more slowly at the end. During the reverse B-to-Q transition the anchor spark disappears and the drift ceases.

Drifting subpulses are traditionally used as a voltmeter to measure the gradient of accelerating potential across the polar cap (van Leeuwen & Timokhin 2012). Assuming a small degree of aliasing in the B-, Tb- and Tq-modes, the large and fast fractional change of P_3 in the Tb- and Tq-modes (comparing to the more gradual smaller change over the course of B-mode) means some rapid and powerful magnetospheric current rearrangements.

The timescales of mode switching for PSR B0943+10 and other mode-switching pulsars are much larger than characteristic time scales of force-free magnetospheres ($\sim P_1$). It has been conjectured that mode switching are a manifestation of metastable magnetospheric states, produced by non-linear interaction between the neutron star magnetic fields, polar cap cascades and current sheets (Timokhin 2010). In particular, these quasi-stable states can have different open fieldline zone sizes and/or different current density distributions within the open field line zone. If switches between the B- and Q-mode are accompanied by a shrinking or expanding of the open field line zone (“polar cap”, for dipole external magnetic field), then, assuming that the radio emission comes from the last open field lines one may infer the polar cap radius from the width of profiles in the B- and Q-modes. Taking 0.06 of spin phase for the former and 0.05 for the latter, for the plausible ranges of the inclination angle and LOS impact angle (Bilous 2018), one may infer a 5% shrinking of the polar cap radius in the Q-mode. According to Timokhin (2010) such change would correspond to a 20% change in spin-down rate between the B- and Q-modes. This change is not possible to detect directly for the 3×10^{-15} s/s spin down rate of PSR B0943+10 considering that mode switching happens on a timescale of hours. However, if the relative fraction of Q- and B-modes change slowly over time, this would have influence on the overall spin-down rate. A similar effect was detected for PSR

B1828–11, where a variable rate of mode transitions were directly related to the spin-down changes (Stairs et al. 2019).

Our crude estimate above implies that the size of polar cap (PC) is larger in the B-mode. Rigoselli et al. (2019) performed direct fitting of the mode-separated thermal X-ray spectra and lightcurves. Generally, the Q-mode has larger polar cap size and larger temperature than B-mode, however the error contours do permit 5% larger PCs radius in B-mode. For this, Q-mode PCs should have about a 20% higher temperature.

On the other hand, Szary et al. (2015) proposed that mode switching reflects switching between two kinds of partially screened gap, with different pair production and a gap screening mechanism. For both kinds the PC temperature should be roughly the same in order to maintain the thermostat mechanism of the partially screened gap. This also does not contradict the results of Rigoselli et al. (2019), although in this case the size of PC in the Q-mode should be larger. We must note that the heating patterns are generally poorly known and the PC is almost certainly not illuminated uniformly. Radio emission may also be a poor indicator of the PC size, coming from the same field lines in both modes but shifting in height.

So far both transitive modes exhibited quite large variations of properties from one session to another. In order to deepen our understanding of the carousel formation, more mode instances should be explored, preferably in a wide frequency range.

Acknowledgements. AB acknowledges the support from the European Research Council under the European Union’s Seventh Framework Programme (FP/2007-2013)/ERC Grant Agreement No. 617199 (‘ALERT’) and Vici research programme ‘ARGO’ with project number 639.043.815, financed by the Dutch Research Council (NWO).

References

- Backer, D. C., Rankin, J. M., & Campbell, D. B. 1975, *ApJ*, 197, 481
 Backus, I., Mitra, D., & Rankin, J. M. 2010, *MNRAS*, 41, 30
 Backus, I., Mitra, D., & Rankin, J. M. 2011, *MNRAS*, 418, 1736
 Bartel, N., Morris, D., Sieber, W., & Hankins, T. H. 1982, *ApJ*, 258, 776
 Bilous, A. V. 2018, *A&A*, 616, A119
 Bilous, A. V., Hessels, J. W. T., Kondratiev, V. I., et al. 2014, *A&A*, 572, A52 (B14)
 Cordes, J. M. 2013, *ApJ*, 775, 47
 Deshpande, A. A. & Rankin, J. M. 2001, *MNRAS*, 322, 438 (DR01)
 Edwards, R. T. & Stappers, B. W. 2003, *A&A*, 410, 961 (ES03)
 Esamdin, A., Lyne, A. G., Graham-Smith, F., et al. 2005, *MNRAS*, 356, 59
 Gil, J. A. & Sendyk, M. 2000, *ApJ*, 541, 351
 Hermsen, W., Hessels, J. W. T., Kuiper, L., et al. 2013, *Science*, 339, 436
 Mereghetti, S., Kuiper, L., Tiengo, A., et al. 2016, *ApJ*, 831, 21
 Miles, M. T., Shannon, R. M., Bailes, M., et al. 2021, *MNRAS*
 Rajwade, K. M., Perera, B. B. P., Stappers, B. W., et al. 2021, *MNRAS*, 506, 5836
 Rankin, J. M. 1983, *ApJ*, 274, 333
 Rankin, J. M., Olszanski, T. E. E., & Wright, G. A. E. 2020, *ApJ*, 890, 151
 Rankin, J. M. & Suleymanova, S. A. 2006, *A&A*, 453, 679
 Rigoselli, M., Mereghetti, S., Turolla, R., et al. 2019, *ApJ*, 872, 15
 Ruderman, M. A. & Sutherland, P. G. 1975, *ApJ*, 196, 51
 Shabanova, T. V., Pugachev, V. D., & Lapaev, K. A. 2013, *ApJ*, 775, 2
 Stairs, I. H., Lyne, A. G., Kramer, M., et al. 2019, *MNRAS*, 485, 3230
 Stappers, B. W., Hessels, J. W. T., Alexov, A., et al. 2011, *A&A*, 530, A80
 Suleymanova, S. A. & Izvekova, V. A. 1984, *Soviet Ast.*, 28, 32
 Suleymanova, S. A., Izvekova, V. A., Rankin, J. M., & Rathnasree, N. 1998, *Journal of Astrophysics and Astronomy*, 19, 1
 Suleymanova, S. A., Kazantsev, A. N., Rankin, J. M., & Logvinenko, S. V. 2021, *MNRAS*, 502, 6094
 Suleymanova, S. A., Logvinenko, S. V., & Smirnova, T. V. 2012, *Astronomy Reports*, 56, 207
 Suleymanova, S. A. & Pugachev, V. D. 2017, *Astronomy Reports*, 61, 428
 Suleymanova, S. A. & Rankin, J. M. 2009, *MNRAS*, 396, 870
 Suleymanova, S. A. & Rodin, A. E. 2014, *Astronomy Reports*, 58, 796
 Szary, A., Melikidze, G. I., & Gil, J. 2015, *MNRAS*, 447, 2295
 Taylor, J. H. & Huguenin, G. R. 1971, *ApJ*, 167, 273
 Timokhin, A. N. 2010, *MNRAS*, 408, L41

- van Haarlem, M. P., Wise, M. W., Gunst, A. W., et al. 2013, *A&A*, 556, A2
 van Leeuwen, A. G. J., Stappers, B. W., Ramachandran, R., & Rankin, J. M. 2003, *A&A*, 399, 223
 van Leeuwen, J. & Timokhin, A. N. 2012, *ApJ*, 752, 155
 Vitkevich, V. V., Alekseev, Y. I., Zhuravlev, V. F., & Shitov, Y. P. 1969, *Nature*, 224, 49
 Wang, N., Manchester, R. N., & Johnston, S. 2007, *MNRAS*, 377, 1383
 Wen, Z. G., Yan, W. M., Yuan, J. P., et al. 2020, *ApJ*, 904, 72